CLAS Note 91-012

A Guide to the Optics of the Tagged Photon Magnet

Daniel I. Sober

Catholic University of America
Washington, DC 20064
10 June 1991

Abstract

This note describes the beam optics of the Hall B Tagged Photon Magnet, whose design is now fixed by the May 1991 bid package. It includes tables and figures which will be useful primarily to those designing the detectors for the Tagged Photon system.

1. Introduction

The CEBAF Hall B Tagged Photon magnet is a modified Elbek-type spectrometer with a full-energy radius of curvature of 11.80 m and a full-energy deflection angle of 30 degrees. The magnet is 6.06 m long with a 6.0 cm gap, and weighs approximately 150,000 pounds. At the nominal maximum energy of 4 GeV, the magnetic field in the gap is 1.13 T. If a suitable power supply is available, the magnet can be run at 1.70 T to provide 6 GeV operation at somewhat degraded field uniformity.

Figure 1 shows the overall layout and dimensions of the system. The field boundary is nearly coincident with the edge of the pole root. The magnet poles will be inside the vacuum system. A stainless steel vacuum chamber, welded to the magnet poles, will extend down to a flange supporting a thin exit window which is as close as possible to the detector plane.

An incident electron beam of energy E_0 strikes a thin radiator foil located a distance D_0 = 0.5 m upstream of the magnet entry edge. Photons of all energies $k < E_0$ are produced at nearly forward angles, and exit through a beam pipe which extends through a hole in the magnet return yoke. The residual electrons, of energy E_0-k, are analyzed by the tagger magnet. It is desired to have the ability to tag photons over the energy range $0.2 < k/E_0 < 0.95$, although not necessarily over the entire range in each experiment.

The deflection angles of detected electrons vary from 48.4° at $k/E_0 = 0.95$ to 31.7° at $k/E_0 = 0.20$. The focal surface is nearly linear, and can be approximated by a flat surface with no significant loss of energy resolution. For the nominal radiator position, the distance from the field boundary to the focal plane varies from 0.46 m at $k/E_0 = 0.95$ to 5.01 m at $k/E_0 = 0.20$. For these photon energy limits, the length of the focal plane is 9.17 m. The detected electrons cross the focal plane at a shallow angle which varies from 26° at $k/E_0 = 0.95$ to 9.3° at $k/E_0 = 0.20$.

Tables I, II and III give the most important details of the focal plane geometry as a function of photon energy and radiator position. They contain much more information than any single user is likely to need. The following text will refer to these tables as required. See the table annotations for additional information.

2. Counter positions and sizes

The dispersion of the system is such that an increment in photon

energy of 1 percent of E_0 results in a displacement of approximately 12 cm along the focal plane. The system is expected to be instrumented for a momentum channel width no finer than 0.2%, which implies a spacing of at least 2.4 cm between detector channels. Because of the grazing angle of traversal, attention must be paid to the variation of this angle along the focal plane, as may be seen in Figure 2. The positions where the various rays cross the focal plane are given in Table I, and the crossing angle θ_{cross} is given in Table II. (Table III gives additional beam optics parameters related to the quantities listed in Tables I and II.)

The transverse width of the counters should ideally be large enough to detect any electron which is transmitted through the magnet gap. The column y_{max} in Table II shows that a half-width of 11.4 cm will cover this region in all cases. Restricting this size to ±10.2 cm (i.e. an 8-inch counter width) would lose only a negligible number of electrons even at E_0 = 0.8 GeV, because in all cases in which y_{max} exceeds 10.2 cm, the characteristic transverse electron spread (y_{char}) is at least a factor of 4 smaller. Since y_{char} is inversely proportional to E_0, the transverse dimensions could be made considerably smaller without sacrificing efficiency at incident energies greater than 0.8 GeV. Figure 3 shows how the detection fraction converges as a function of transverse detector size -- note that $_y$char = $\theta_{ce} \times R_{34}$ of Table III.

3. Polarized photon considerations -- radiator position

Linearly polarized photons can be tagged by placing a transverse cut on the position of the electron at the focal plane which defines the transverse angle of the electron to the order of 1 θ_{ce}, where the "electron characteristic angle" θ_{ce} is defined by

$$\theta_{ce} = (m_e/E_0)\ k/(E_0-k)\,.$$

The dynamics of the bremsstrahlung process are such that this effect yields appreciable polarization only for photon energies $k < 0.5\ E_0$, so only the lower part of the focal plane can be used.

Because the flux falls rapidly with angle at angles greater than θ_{ce}, it is sufficient to impose a one-sided right or left cut, excluding electrons from the region around y=0. Making use of this effect will require moving the detectors away from the central axis of the focal plane by distances of the order of 1-4 mm for $0.2 < k/E_0 < 0.8$ at E_0 = 0.8 GeV (see column y_{char} in Table II).

Since the transverse distance corresponding to θ_{ce} is inversely

proportional to E_0, the displacement required for a particular level of polarization becomes extremely small at incident energies above 2 GeV. This can be partially compensated by increasing the radiator-to-magnet distance D_0 from its "normal" value of 0.5 m. Table II shows that increasing D_0 to 10 m increases the characteristic transverse displacement y_{char} by about a factor of 3 in the useful part of the focal plane. Varying the radiator position would keep the transverse displacements to a manageable size even at high E_0.

Figure 4 shows in more detail how y_{char} varies with radiator distance. The solid circle in each part indicates the value for E_0 = 0.8 GeV at the normal distance of 0.5 m.

4. Energy resolution

The energy resolution of the system is reasonably constant as a fraction of the incident energy E_0. Unless otherwise noted, "energy resolution" will refer to one standard deviation in k/E_0. The principal contributions to the energy resolution, assuming arbitrarily good position resolution at the focal plane, are:

a) For the "normal" radiator position (D_0 = 0.5 m), the resolution is limited by multiple scattering in the exit window of the vacuum chamber, and can be made better than 0.1% with a reasonable choice of window. (See section 6).

b) For the "far-upstream" radiator position (D_0 = 10 m) which may be used for polarization at high energy, the dominant effect is the "first-order" contribution to the resolution which results from keeping the detector plane fixed while the true focal surface moves inward. This degrades the resolution by 0.2% (1σ) in the worst case.

c) Linearizing the focal plane has negligible effect on the resolution for normal radiator position (<.02% at E_0 = 0.8 GeV, scaling as $1/E_0$). Second-order optical effects are even smaller (<.005% at 0.8 GeV).

Non-uniformity in the achieved magnet field will probably have effects more important than those of (c), but no attempt has been made to estimate it.

5. Tagging efficiency and collimation losses

The 6-cm-wide magnet gap limits the fraction of the electron cone which arrives at the detector plane. For the normal radiator

position (D_0 = 0.5 m), the loss of electrons is very small, exceeding 2.5% only for $k/E_0 > 0.9$ and $E_0 < 1.6$ GeV (Figure 6).

For the far-upstream radiator position (D_0 = 10 m), electron losses are larger but at energies above 1.6 GeV they remain at the few-percent level in the region of the focal plane which is useful for polarization measurements ($k/E_0 < 0.5$).

A different but related question is the fraction of tagged photons which strike the CLAS target. The characteristic photon production angle is $\theta_c = m_e/E_0$. Because of the large distance (≈22 m) from radiator to target, only about 55% of the photons produced by a 0.8-GeV electron beam will strike a 4-cm-diameter target. Figure 5 shows this fraction as a function of endpoint energy and target diameter; it is nearly independent of k/E_0. The photons outside the target diameter will normally be collimated out, to prevent unwanted interactions with the target mountings and other hardware.

6. Exit window

As noted in Section 4, multiple scattering in the exit window of the vacuum chamber is probably the major limitation on resolution, although for the desired energy channel width the limitations are not severe. Figure 7 shows the geometrical considerations. We assume that the exit window is attached to a flange which is parallel to the detector plane and as close as possible to it. The electrons traverse the exit window foil at a grazing angle θ_{cross} and continue to the detector plane. Their distance of travel to the detector plane is $d_{exit}/\sin\theta_{cross}$, and the projection of the multiple scattering angle over this distance leads to a momentum uncertainty which depends on the dispersion in that region of the focal plane.
Hall Crannell has investigated the strength, deformation and availability of various materials for the exit window. Over a 20-cm span, he finds that the minimum safe thickness of almost any suitable material is likely to deform by about 4 cm under vacuum. Thus it is unlikely that the foil-to-detector distance (measured from the point of maximum deflection, where most of the electrons traverse it) can be made smaller than about 6 cm.

Table IV lists the multiple-scattering contributions to the resolution, under the assumption that a 0.00357-radiation-length (0.005") titanium window is used. With a foil-to-detector distance of 6 cm, the largest contribution is 0.10% (1σ) at E_0 = 0.8 GeV and $k/E_0 = 0.8$; the results scale as $1/E_0$ and as the square root of the foil thickness in radiation lengths.

Multiple scattering in the foil contributes not only to the energy resolution but also to the transverse angle resolution

needed for polarization tagging (Section 3 above.) For the .005" titanium foil assumed above, the ratio of multiple scattering (1σ) to θ_{ee} varies from .37 to .20 for $0.2 < k/E_0 < 0.8$, independent of E_0, so that it is possible (barely) to discriminate on the level of 1 θ_{ee}.

It may be possible to improve these results by up to a factor of 3 by using a carbon-fiber composition window. This would clearly be beneficial to the polarization program.

7. Summary

The current design for the tagger magnet provides for an energy resolution in "normal" mode of 0.1% (1σ in k/E_0) at $E_0 = 0.8$ GeV, scaling as $1/E_0$. (In the "polarization" mode, the resolution will be somewhat worse if large displacements of the target position are employed.) This resolution could be improved by a factor of 2 to 3 if a suitable composition window can be built.

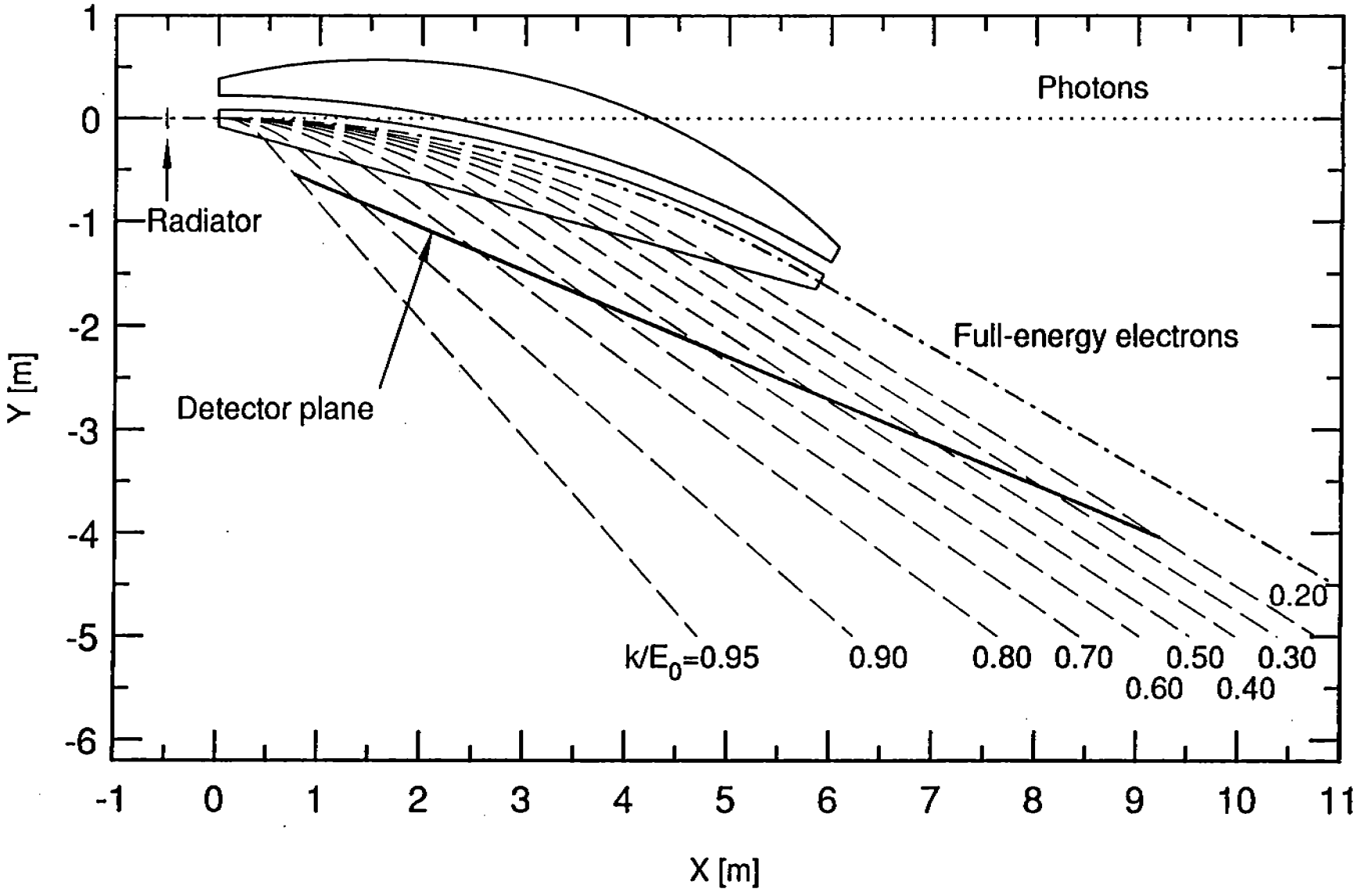

Figure 1. Elevation view of the magnet, detector plane, and selected electron trajectories. The origin of the coordinate system is at the point where the incident beam enters the magnet field.

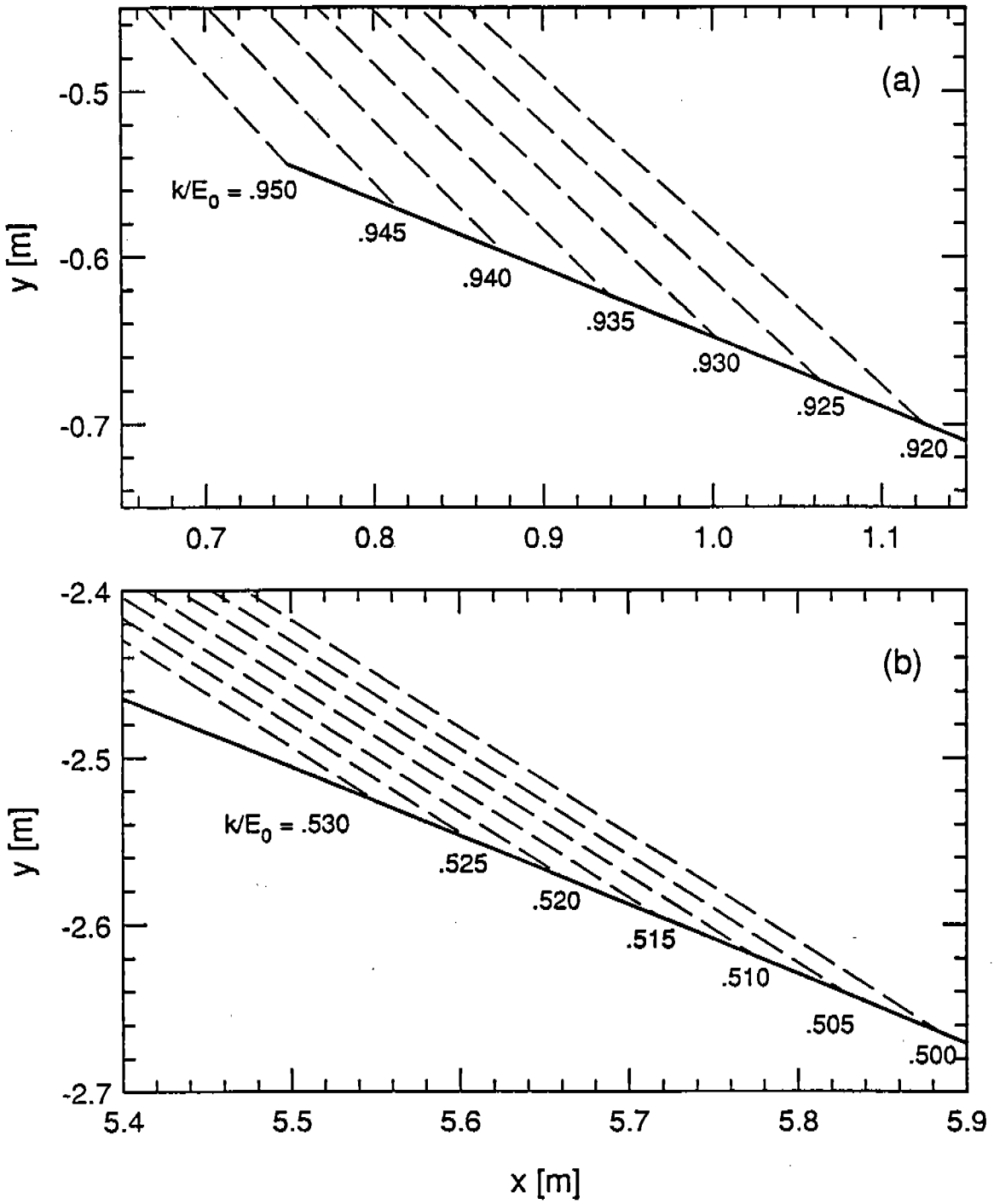

Figure 2. Geometry of electron trajectories separated in energy by 0.5% of E_0 intersecting the detector plane. **(a)** Near the maximum tagged photon energy, $k/E_0 = 0.95$. **(b)** Near $k/E_0 = 0.50$.

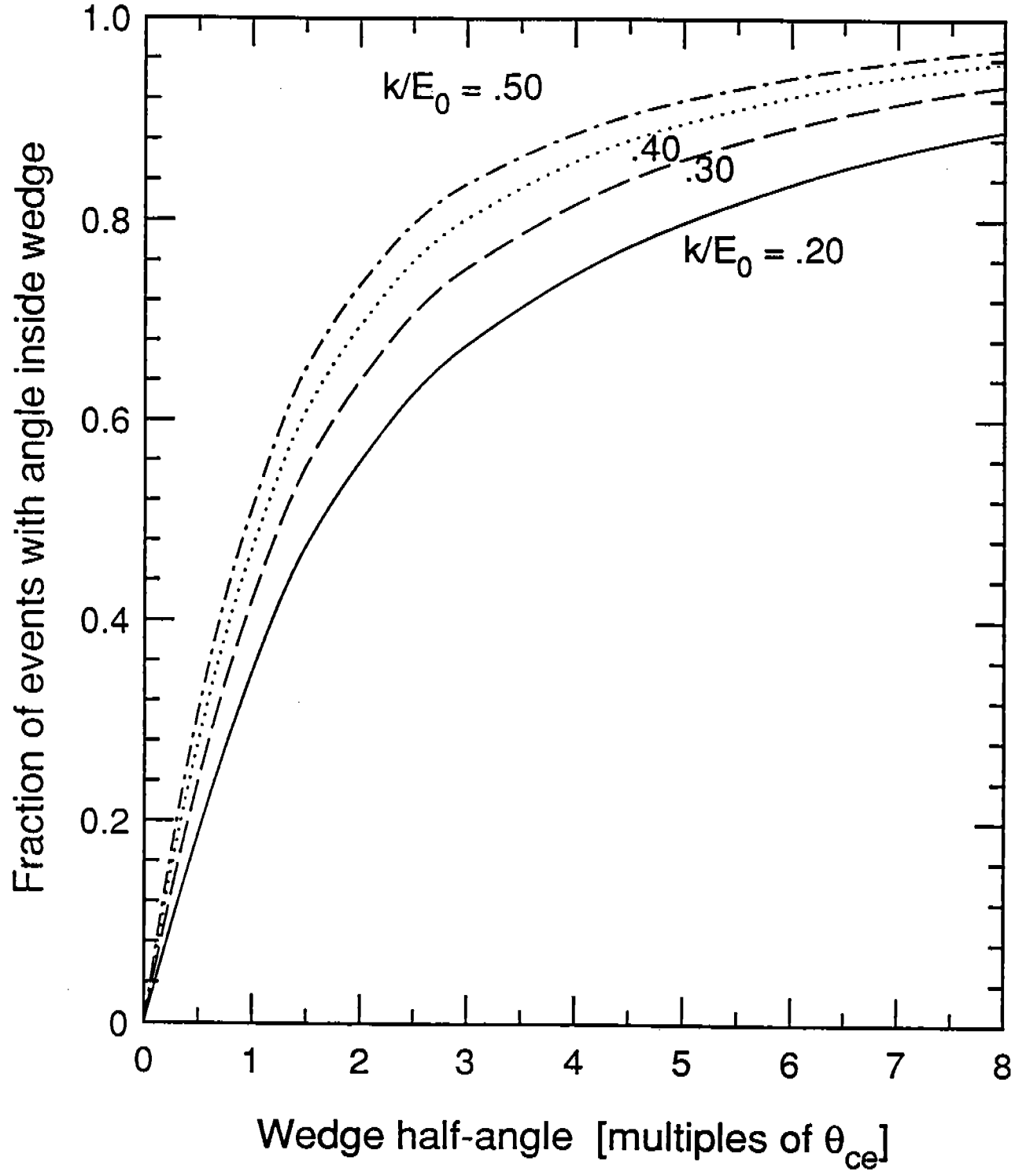

Figure 3. Fraction of bremsstrahlung events whose electron falls within an angular "wedge" of given half-angle in units of θ_{ce}. This can be related to the fraction passing through the magnet gap by the factor R_{34B}, and to the fraction within a given detector width by the factor R_{34} (both in Table III.)

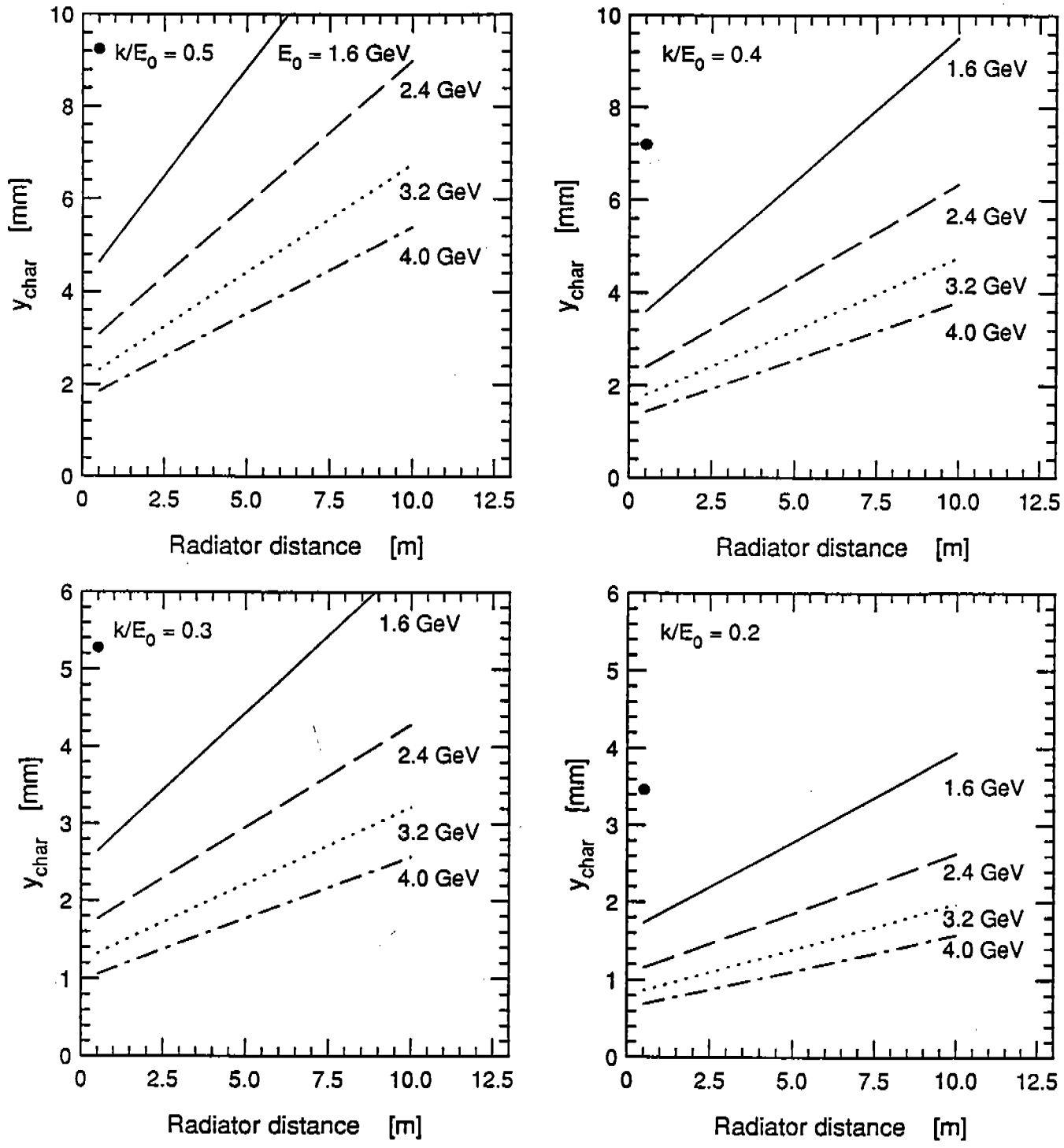

Figure 4. Characteristic transverse position at the focal plane y_{char} as a function of radiator distance. The solid circle • represents the value for 0.8 GeV at the normal radiator distance of 0.5 m.

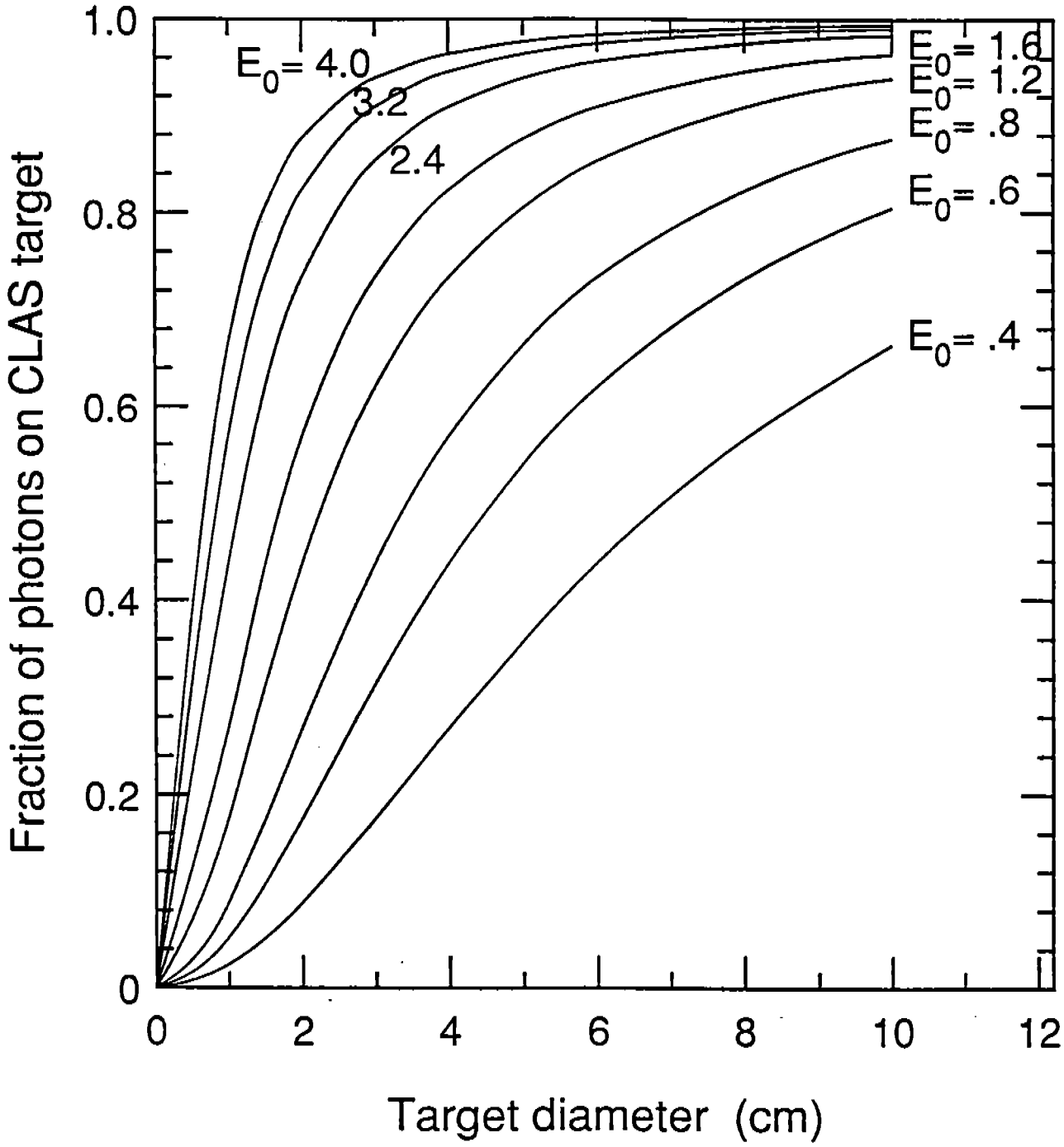

Figure 5. Fraction of bremsstrahlung photons incident on the CLAS target as a function of target diameter (assuming distance from radiator = 22 m). Each curve is labeled by th endpoint energy in GeV. (Results are calculated for $k/E_0 = 0.8$, but are independent of k/E_0 to within ≈3%).

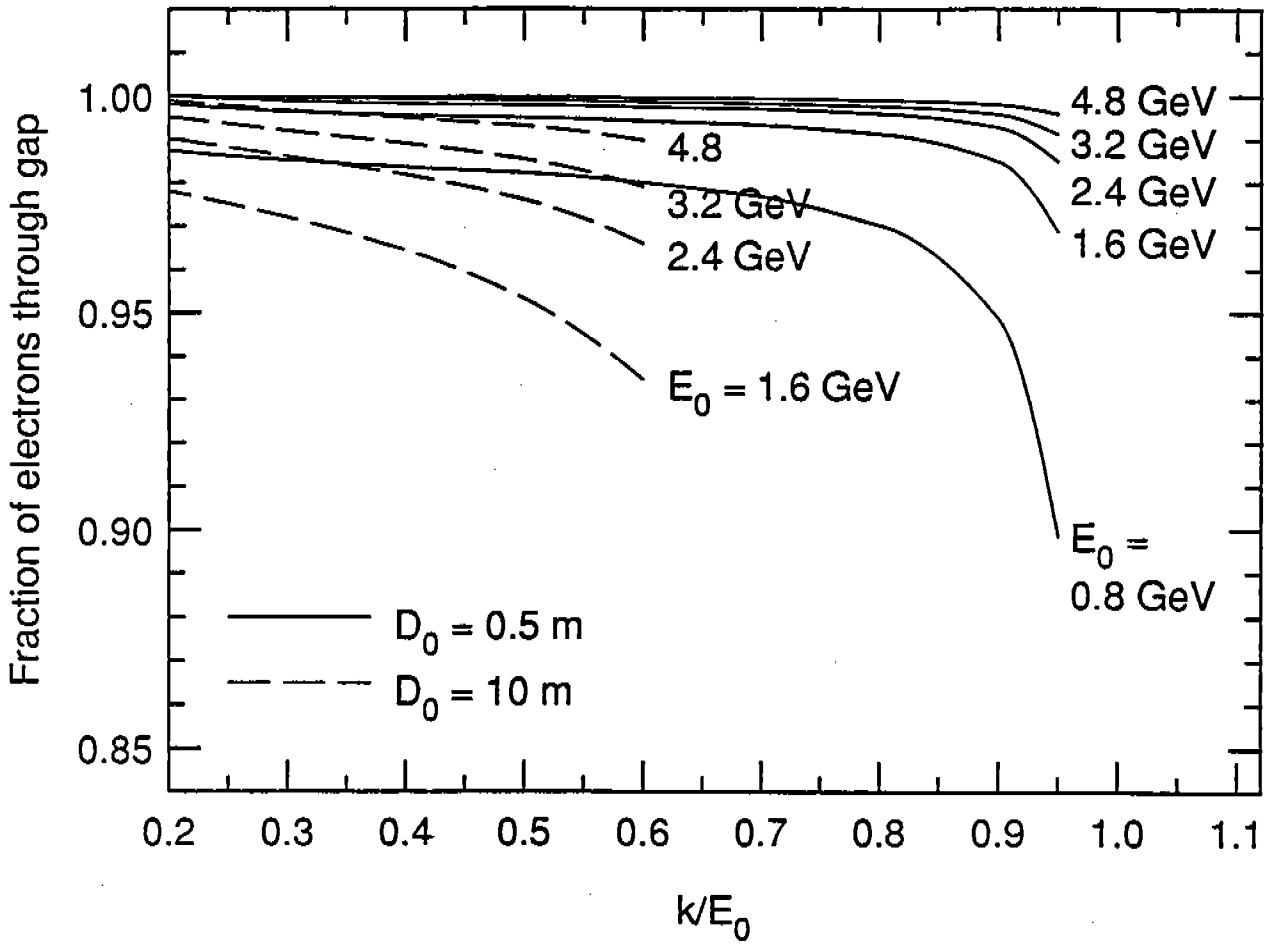

Figure 6. Fraction of electrons reaching the detector plane through the 6-cm magnet gap, as a function of k/E_0, for various values of E_0. **Solid curves** = normal radiator position. **Dashed curves** = extreme upstream radiator position.

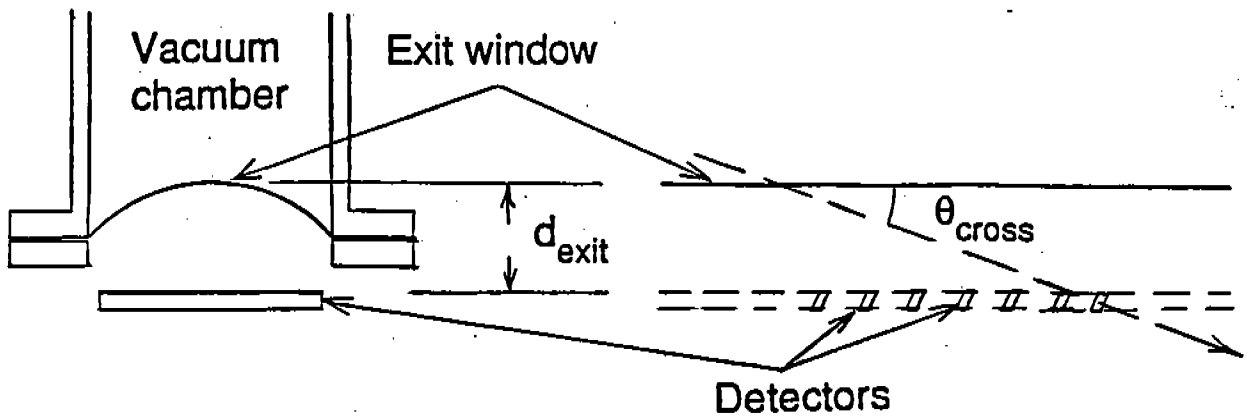

Figure 7. Geometry of the exit window region, shown in two perpendicular views. The closest distance between the exit window and the detector plane, d_{exit}, is equal to the vacuum deflection of the window foil and an additional distance required for the counters to clear the flange. θ_{cross} varies with k/E_0 and is given in Table II.

Table I.
Data useful for layout of the focal plane detectors.
The radiator position is D_0 = 0.5 m, and the entry edge is normal to the incident beam direction. The detector plane (also referred to as "focal plane" is defined by the straight line

$$Y = -3.1248 - (X - 7.0000) \tan(22.4285°)$$

in the coordinate system of Figure 1, which has been fit to the true focal surface for $0.2 < k/E_0 < 0.8$.
All values in this table are independent of E_0.

Explanation of symbols:

- k/E_0 = photon energy as a fraction of incident energy
- p/E_0 = electron energy as a fraction of incident energy
- θ_{bend} = deflection angle of electron in field
- D_2 = distance from field boundary to detector plane
- X_E, Y_E = coordinates of exit point (where electron crosses field boundary) in coordinate system of Figure 1
- X_{FP}, Y_{FP} = coordinates of electron intersection with detector plane in coordinate system of Figure 1
- d_{FP} = distance along detector plane (relative to k/E_0 = .95)

k/E_0	p/E_0	θ_{bend} (deg)	D_2 (m)	X_E (m)	Y_E (m)	X_{FP} (m)	Y_{FP} (m)	d_{FP} (m)
.95	.05	48.39	.463	.441	-.198	.749	-.545	.000
.90	.10	40.78	.784	.771	-.287	1.364	-.799	.666
.80	.20	36.06	1.399	1.390	-.452	2.520	-1.276	1.916
.70	.30	34.25	2.004	1.992	-.614	3.649	-1.742	3.137
.60	.40	33.28	2.606	2.590	-.774	4.768	-2.204	4.348
.50	.50	32.67	3.207	3.185	-.933	5.884	-2.664	5.556
.40	.60	32.25	3.807	3.778	-1.092	6.998	-3.124	6.760
.30	.70	31.95	4.407	4.371	-1.251	8.110	-3.583	7.964
.20	.80	31.72	5.007	4.963	-1.410	9.222	-4.042	9.166

Table II.
Data on acceptance, dispersion and resolution.
The radiator position is either D_0 = 0.5 m ("normal" mode) or D_0 = 10 m (polarization mode), and the entry edge is normal to the incident beam direction. The detector plane is as described in Table I.

Explanation of symbols:

- F_{acc} = Fraction of electrons accepted through the magnet gap (gap half-width = 3 cm)
- y_{char} = Transverse position at detector plane corresponding to θ_{ce} (electron characteristic angle defined in text)
- y_{max} = Transverse position at detector plane of electron which just clears the magnet gap (half-width 3 cm)
- θ_{cross} = Angle at which electron crosses detector plane
- D_{perp} = Dispersion perpendicular to the electron path (cm per percent of E_0)
- D_{long} = Disperson along the detector plane (cm per percent of E_0)
- $\delta k^1/E_0$ = First-order contribution to resolution due to difference between detector plane and true focal plane (1σ in k/E_0)
- * = Calculated for E_0 = 0.8 GeV; scales as $1/E_0$
- ** = Calculated for E_0 = 0.8 GeV; see Figure 3

k/E_0	F_{acc} **	y_{char} (mm) *	y_{max} (mm)	θ_{cross} (deg)	D_{perp} (cm/%)	D_{long} (cm/%)	$\delta k^1/E_0$ (%) *
D_0 = 0.5 m (Normal mode)							
.9500	.8985	39.670	96.16	25.961	6.170	14.094	-.0211
.9000	.9487	26.693	103.26	18.356	4.046	12.848	-.0063
.8000	.9702	18.357	108.34	13.635	2.899	12.295	-.0007
.7000	.9767	14.369	110.45	11.820	2.488	12.147	.0001
.6000	.9800	11.562	111.62	10.848	2.275	12.087	.0002
.5000	.9822	9.249	112.38	10.240	2.143	12.057	.0001
.4000	.9837	7.190	112.90	9.823	2.054	12.039	.0001
.3000	.9852	5.279	113.29	9.520	1.989	12.029	.0000
.2000	.9874	3.462	113.59	9.288	1.940	12.021	.0000
D_0 = 10 m (Polarization mode)							
.5000	.8703	27.012	94.72	10.240	2.143	12.057	-.2010
.4000	.8994	19.019	95.64	9.823	2.054	12.039	-.1426
.3000	.9194	12.876	96.48	9.520	1.989	12.029	-.0962
.2000	.9333	7.890	97.25	9.288	1.940	12.021	-.0582

Table III.
Data useful for TRANSPORT/RAYTRACE calculations, and first-order transport matrix elements.
The radiator position is either D_0 = 0.5 m ("normal" mode) or D_0 = 10 m (polarization mode), and the entry edge is normal to the incident beam direction. The detector plane is as described in Table I.

Explanation of symbols: (R_{ij} = transport matix elements)

θ_2	=	angle of exit edge relative to outgoing electron direction
ℓ_{arc}	=	arc length of electron path inside field
D_2	=	distance from exit edge to detector plane
R_{34E}	=	$(y\|y')$ from radiator to exit edge
R_{11}	=	$(x\|x)$ from radiator to detector plane
R_{12}	=	$(x\|x')$ from radiator to detector plane
R_{16}	=	$(x\|p)$ from radiator to detector plane
R_{33}	=	$(y\|y)$ from radiator to detector plane
R_{34}	=	$(y\|y')$ from radiator to detector plane

Note that the momentum of the electron which is being transported through the magnet is E_0-k. The entry edge angle is θ_1 = 0°, the half-width of the magnet gap is 3.0 cm, and the field index is 0.

k/E_0	θ_2 (deg)	ℓ_{arc} (m)	D_2 (m)	R_{34E} (mm/mr)	R_{11}	R_{12} (mm/mr)	R_{16} (cm/%)	R_{33}	R_{34} (mm/mr)
D_0 = 0.5 m (Normal mode)									
.95	-56.611	.498	.463	1.021	-.715	-.134	.308	2.889	3.269
.90	-64.216	.840	.784	1.349	-.719	-.055	.405	2.923	4.643
.80	-68.937	1.485	1.400	1.989	-.785	-.010	.580	2.937	7.185
.70	-70.751	2.116	2.004	2.619	-.832	.003	.747	2.935	9.641
.60	-71.724	2.741	2.606	3.243	-.864	.007	.910	2.931	12.07
.50	-72.332	3.364	3.207	3.866	-.888	.006	1.072	2.927	14.48
.40	-72.748	3.985	3.807	4.487	-.906	.003	1.232	2.924	16.89
.30	-73.052	4.606	4.407	5.107	-.919	-.002	1.393	2.921	19.29
.20	-73.284	5.226	5.007	5.726	-.930	-.007	1.552	2.919	21.68
D_0 = 10 m (Polarization mode)									
.50	-72.332	3.364	3.207	13.393	-.888	-8.429	1.072	2.927	42.29
.40	-72.748	3.985	3.807	14.009	-.906	-8.600	1.232	2.924	44.66
.30	-73.052	4.606	4.407	14.626	-.919	-8.735	1.393	2.921	47.04
.20	-73.284	5.226	5.007	15.243	-.930	-8.846	1.552	2.919	49.41

Table IV
Exit window multiple-scattering contribution (1σ) to tagger energy resolution, given in percent of E_0. Also
"Transv. ratio" = (y_{rms} due to multiple scattering)/y_{char}
where y is the transverse coordinate at the detector plane and y_{char} is defined in Table II.

Two cases are calculated: .006" titanium foil, and .006" carbon composition. t is the foil thickness in radiation lengths; d_{exit} is defined by Figure 4.

t (R.L)	d_{exit} (cm)	k/E_0	$\delta k/E_0$ (percent) E_0 (GeV) = .800	1.600	2.400	3.200	4.000	Transv. ratio
Titanium, .005 inches:								
.00357	6.0	.950	.0751	.0375	.0250	.0188	.0150	.117
		.900	.0936	.0468	.0312	.0234	.0187	.142
		.800	.1016	.0508	.0339	.0254	.0203	.161
		.700	.0973	.0487	.0324	.0243	.0195	.169
		.600	.0909	.0454	.0303	.0227	.0182	.179
		.500	.0843	.0422	.0281	.0211	.0169	.195
		.400	.0776	.0388	.0259	.0194	.0155	.221
		.300	.0717	.0359	.0239	.0179	.0143	.270
		.200	.0668	.0334	.0223	.0167	.0134	.374
Carbon composition, .006 inches:								
.00080	4.5	.950	.0267	.0133	.0089	.0067	.0053	.041
		.900	.0332	.0166	.0111	.0083	.0066	.050
		.800	.0361	.0180	.0120	.0090	.0072	.057
		.700	.0345	.0173	.0115	.0086	.0069	.060
		.600	.0323	.0161	.0108	.0081	.0065	.063
		.500	.0299	.0150	.0100	.0075	.0060	.069
		.400	.0275	.0138	.0092	.0069	.0055	.078
		.300	.0255	.0127	.0085	.0064	.0051	.096
		.200	.0237	.0119	.0079	.0059	.0047	.133